Fast Energy Relaxation by Trap States Decreases Electron Mobility in TiO2 Nanotubes: Time-Domain Ab Initio Analysis

ARTICLE *in* JOURNAL OF PHYSICAL CHEMISTRY LETTERS · APRIL 2014

Impact Factor: 7.46 · DOI: 10.1021/jz500565v

6 AUTHORS, INCLUDING:

Zhenyu Guo
Soochow University (PRC)
13 PUBLICATIONS **75** CITATIONS
SEE PROFILE

Oleg Prezhdo
University of Rochester
306 PUBLICATIONS **6,778** CITATIONS
SEE PROFILE

Tingjun Hou
Zhejiang University
241 PUBLICATIONS **4,621** CITATIONS
SEE PROFILE

THE JOURNAL OF PHYSICAL CHEMISTRY Letters

Letter

pubs.acs.org/JPCL

Fast Energy Relaxation by Trap States Decreases Electron Mobility in TiO_2 Nanotubes: Time-Domain Ab Initio Analysis

Zhenyu Guo,[†] Oleg V. Prezhdo,[‡] Tingjun Hou,[†] Xue Chen,[†] Shuit-Tong Lee,[†] and Youyong Li*,[†]

[†]Institute of Functional Nano & Soft Materials (FUNSOM), Collaborative Innovation Center of Suzhou Nano Science and Technology, Soochow University, Suzhou, Jiangsu 215123, China

[‡]Department of Chemistry, University of Rochester, Rochester, New York 14642, United States

ABSTRACT: Highly ordered TiO_2 nanotube arrays can be grown by simple electrochemical anodization of a titanium metal sheet, stimulating intense research and applications to solar cells and fuels. TiO_2 nanotubes were expected to exhibit better electron transport than nanocrystal films. However, experiments showed that nanotubes provided little advantage over nanoparticles. Using nonadiabatic molecular dynamics, we demonstrate that oxygen vacancies, which are common in TiO_2, accelerate nonradiative energy losses by an order of magnitude. Oxygen vacancies produce localized Ti^{3+} states hundreds of millielectronvolts below the TiO_2 conduction band. The states lower the nanotube band gap, trap excited electrons, induce stronger electron−phonon couplings, and facilitate the relaxation. Our results rationalize the unforeseen experimental observations and provide the atomistic basis for improving the structure and charge transport by TiO_2 nanotubes.

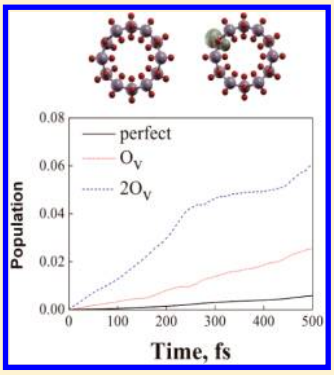

SECTION: Physical Processes in Nanomaterials and Nanostructures

Dye-sensitized solar cell (DSSC) is a promising photovoltaic device avoiding the use of silicon. It has high efficiency and low cost.[1−5] The power conversion exceeds 12% for Co-porphyrin sensitized solar cells[6] and 15% for perovskite-sensitized photovoltaic systems.[7] DSSC performance can be improved further by inhibiting recombination of injected electrons with oxidized dye molecules and electrolyte species. Slow electron transport limits electron collection efficiency and lowers DSSC performance, by allowing more time for electron loss inside TiO_2 and at the TiO_2−electrolyte interface. Electrons trapped by defects throughout the TiO_2 network and in the interfacial area reduce charge transport. The trapping mechanism has been extensively investigated by both experiment[8−11] and theory.[12−15]

Since the initial synthesis in 2001,[16] titanium dioxide (TiO_2) nanotubes (NTs) have attracted significant interest due to their potential in applications to photocatalysis, gas sensing, biomedical devices, Li^+ and H_2 storage, as well as DSSC.[17−23] It has been suggested that TiO_2 NTs may improve DSSC performance by allowing directional electron transport, lowering structural disorder, and creating fewer grain boundaries compared with nanoparticle networks and porous anatase films.[24,25] By anchoring pigments or quantum dots to a NT array, one can make TiO_2 NTs respond to visible light, extending the UV photoresponse of pristine TiO_2. It has been expected that free carriers will be transported to the anodic TiO_2 electrode along the NTs, enhancing electron transport relative to the porous nanoparticle film in the traditional DSSC.

Surprisingly, NTs did not demonstrate the expected improvements in the electron mobility over nanoparticle films.[26] The Schmuttenmaer group probed the microscopic free-carrier transport in NTs arrays using time-resolved terahertz spectroscopy (TRTS).[27] TRTS confirmed that the electron mobility was not superior to that of nanoparticle films. In nanoparticles, the energy loss corresponds to a decrease in the backscattering parameter and the electron scattering rate on a 500 fs time scale, while the time scale for phonon-induced relaxation is ∼10−50 times longer in NTs. The slow carrier transport in NTs was attributed to the exciton-like Ti^{3+} trap states, resulting from oxygen vacancies (O_v) generated during vacuum or inert gas annealing in fabrication. The electron transport could be improved when the NTs were annealed in an oxygen-rich environment. Unfortunately, oxygen vacancies cannot be fully eliminated with current fabrication procedures; therefore, one cannot determine experimentally how detrimental the vacancies are to the charge transport. This goal can be achieved in a theoretical study.

The current Letter reports a time-domain ab initio simulation of the electron relaxation (evolution of the LUMO) in TiO_2 NTs with and without oxygen vacancies. The simulation shows that defects accelerate electron losses by an order of magnitude, rationalizing the unexpected lack of enhancement of charge transport by NTs. The defect states are highly localized and therefore have the same influence on the transport, regardless of whether it occurs in NTs or nanoparticle arrays. The simulation provides detailed insights into the structural and dynamical mechanism for the trapping. It shows that oxygen vacancies result in Ti^{3+} sites with energies 0.8 eV below the

Received: March 20, 2014
Accepted: April 21, 2014
Published: April 21, 2014

   dx.doi.org/10.1021/jz500565v | *J. Phys. Chem. Lett.* 2014, 5, 1642−1647

bottom of the TiO_2 conduction band. The localized electronic states create strong electron-vibrational coupling.[28] The fast electron trapping results from the combination of the reduced energy gap and enhanced electron-vibrational coupling. Multiple defects act in a cooperative manner by increasing the coupling further, while having little additional effect on the trap energy. The trap energy is sufficiently small to facilitate fast trapping, while at the same time, it is sufficiently large to prevent the trapped electrons from returning to the TiO_2 conduction band. The study identifies the phonon modes responsible for the relaxation. These modes are polar can be probed by both infrared and Raman experiments.

We perform fully atomistic simulations with the mixed quantum-classical approach[29] that puts nonadiabatic molecular dynamics (NAMD) within the framework of time-dependent density functional theory (TDDFT).[30,31] The light electrons are treated quantum mechanically, while the heavier and slower nuclei are treated semiclassically. The approach has been previously tested and applied to study the electron transfer and relaxation dynamics at the interface of TiO_2 and dye molecules,[32] quantum dots[33] and graphene,[34] in carbon NTs,[35] nanoribbons,[36] graphanes,[37] and metallic nanoclusters.[28]

A single-layer TiO_2 NT can be formed by rolling an anatase (101) sheet along either the [010] or [$\bar{1}$01] direction. Only (n,0) and (0,m) NTs can be constructed due to symmetry restrictions, which is different from that for the well-known carbon NT structures. The (6,0) TiO_2 NT with the 8 Å diameter has been chosen to minimize the simulation cell and electronic basis, as shown in Figure 1. The electronic properties

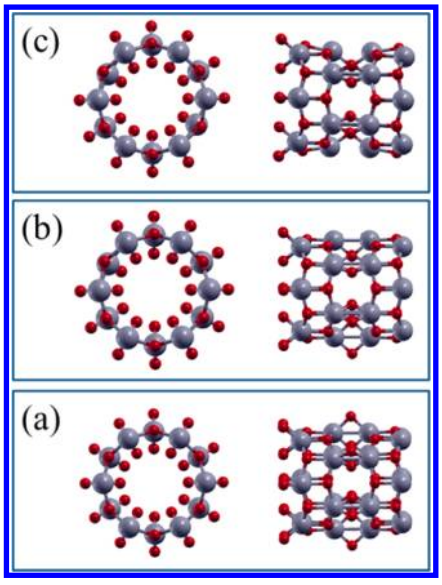

Figure 1. Side and top views of the simulation cell of the (6,0) TiO_2 nanotube for (a) perfect structure, (b) one oxygen-vacancy, and (c) two symmetric oxygen vacancies, optimized at 0 K.

and adiabatic MD are computed with the Vienna ab initio simulation package (VASP)[38] using a plane-wave basis, nonlocal Perdew–Burke–Ernzerhof (PBE) functional[39] and the projector-augmented wave (PAW) description of core electrons.[40,41] Accurate description of Ti^{3+} states can be achieved by hybrid DFT functionals[15,42,43] or DFT+U method.[44–47] Hybrid functionals mix in a part of "exact" Hartree–Fock exchange into the exchange-correlation functionals to ensure localization. In DFT+U method, a function is added to correct the Hamiltonian to mitigate delocalization. We chose DFT+U for all calculations of electronic structure and MD considering computational efficiency. U = 3.3 eV has been employed to investigate the Ti^{3+} electronic states.[48] A U value of 3.3 eV gives defect states around 0.8 to 0.9 eV below the conduction band, whereas a U value of 4.1 eV gives defect states around 1.4 eV. A defect state is observed experimentally at ∼1 eV below the conduction band. Here U = 3.3 eV has been employed to investigated the Ti^{3+} electronic states, which is able to give a reasonable description of band gap. Following the study of the optimized NT, we produce MD trajectories at 300 K. The systems are heated to the required temperature by repeated velocity rescaling. Then, 5 ps adiabatic MD trajectories are generated in the microcanonical ensemble with a 1 fs atomic time step. It should be noted that PBE+U simulations of the dynamics of defects have been performed at the reduced titania TiO_2 (110) surface,[49] and the thermally activated hopping of excess charge between different Ti sites is the focus of their interest. In current work, the MD trajectories are used to sample initial conditions for NAMD, such as energy and nonadiabatic couplings.

The surface of the TiO_2 NT contains two-fold coordinated bridging oxygen O^{2-} ions (O_{2c}) and three-fold coordinated O^{2-} ions (O_{3c}). An NT with an O_{2c} vacancy on the outer surface is chosen as our model (Figure 1b) because its ground-state energy is more favorable than that of the NT with an O_{3c} vacancy. The formation energy of O_{2c} is 0.45 eV lower than that of O_{3c} vacancy. We also consider a NT with two O_{2c} vacancies (Figure 1c).

Figure 2 shows the density of states (DOS) of the TiO_2 NTs with and without defects. Oxygen vacancies create Ti^{3+} trap states 0.86 eV below the bottom of the conduction band (Figure 2b,c), in good agreement with the experimental results for bulk TiO_2 (∼1 eV).[50] Two nearest Ti atoms share the trapped electron pair. The height of the peak corresponding to the defect state is doubled in Figure 2c relative to Figure 2b,

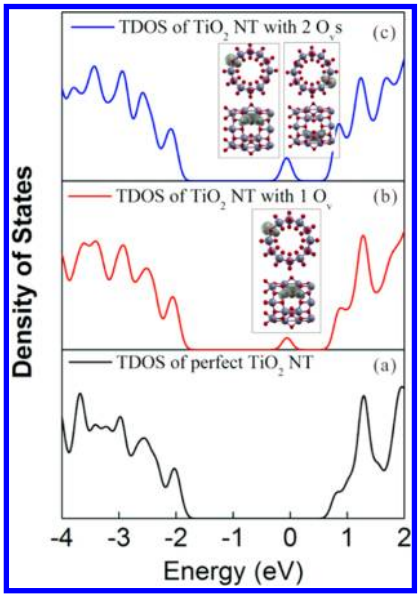

Figure 2. Density of states for (a) perfect TiO_2 nanotube, (b) TiO_2 nanotube with one O_{2c} vacancy, and (c) TiO_2 nanotube with two O_{2c} vacancies in the simulation cell. The inserts show side and top views of the Ti^{3+} states.

dx.doi.org/10.1021/jz500565v | J. Phys. Chem. Lett. 2014, 5, 1642–1647

representing two degenerate Ti^{3+} states below the conduction band. The ground states are singlets for both systems, which is consistent with the situation in bulk anatase.[15] The introduction of the second O_{2c} vacancy has a minor effect on the state energy. The thermally averaged energy gap grows from 0.74 to 0.87 eV (Table 1, Figure 3).

Table 1. Nonradiative Relaxation Time, Average Absolute Nonadiabatic Coupling, and Average Transition Energy for the Three TiO_2 Nanotubes, Figure 1[a]

type	time (ps)	NA coupling (meV)	transition energy (eV)
perfect NT	100	4.45(3.58)	2.27(0.12)
O_v	20	6.44(5.81)	0.74(0.16)
$2O_v$	8.3	10.55(9.66)	0.87(0.15)

[a]Values in the parentheses give fluctuations (root-mean-square deviation) in the nonadiabatic coupling and transition energy.

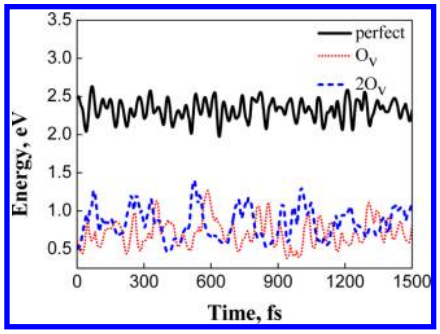

Figure 3. Evolution of the energy gaps for the perfect TiO_2 nanotube (solid black line) and the nanotubes with one O_v defect (red dotted line) and two O_v defects (blue dashed line) at 300 K. The gaps (differences between HOMO−LUMO energy) are from the bottom of the conduction band to the top of the valence band and to the trap states, respectively.

Atomic motions drive fluctuations of the electronic energy levels. The fluctuation amplitude reflects the strength of the electron−phonon coupling. Figure 3 shows the evolution of energy gaps between the bottom of the conduction band and the next lowest state available for the electron. It is the top of the valence band occupied by the hole for the perfect structure, while it is the trap state for the tubes with the O_v and $2O_v$ vacancies. Oxygen defects significantly lower the energy gap that the electron needs to traverse to disappear from the conduction band. The defects also increase the electron−phonon coupling, as reflected in both the absolute value of the NA coupling and the magnitude of the fluctuation of the transition energy (Table 1). Notably, the second defect leads to a significant growth of the NA coupling. Localized defect states increase electron−phonon coupling in most systems, in particular, in carbon NTs.[51]

To elucidate the atomic motions that are responsible for the energy losses, we identify the phonon modes that couple to the electronic subsystem. Figure 4 presents the Fourier transforms (FTs) of the energy gaps shown in Figure 3. The FTs indicate that the electronic transitions involving oxygen vacancies couple to a broader spectrum of lower frequency vibrations than the electronic transition of the perfect NT. The electron relaxation in the ideal NT occurs primarily due to the high and intermediate frequency motions of the Ti−O network, at 490 and 790 cm^{-1}. The defect transitions couple to low-frequency

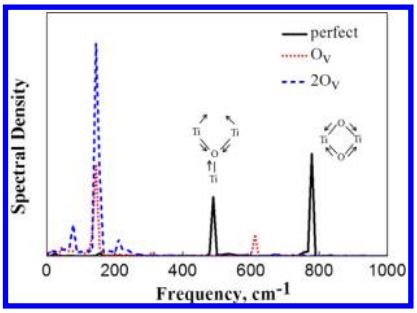

Figure 4. Fourier transforms (FTs) of the evolution of energy gaps shown in Figure 3. The diagrams illustrate the atomic motions that are responsible for the FT peaks. The units used on the *y* axis are the same for all three systems. Electrons in the perfect TiO_2 nanotube relax by coupling to high-frequency phonon modes at 490 and 790 cm^{-1}. Relaxation in the tubes with oxygen defects involves a wider range of vibrations, primarily at low frequency.

modes below 200 cm^{-1}, and the peak intensity for the $2O_v$ case is particularly large.

The exact assignment of the Raman spectra of TiO_2 NTs is not available so far. According to the literature,[52] there are six Raman (A_{1g} + $2B_{1g}$ + $3E_g$) active modes for anatase TiO_2 at 147, 198, 398, 515, 640, and 796 cm^{-1}. The two peaks in the spectra of the perfect NT shown in Figure 4 correspond to the 515 and 796 cm^{-1} modes. The NT spectrum is similar to that of the protonic lepidocrocite titanate;[53] therefore, the identified vibrational may be approximately regarded as a reflection of the titanate structure. The peak at 490 cm^{-1} can be identified as Ti−O bending and stretching vibrations. The 790 cm^{-1} peak is characteristic of the stretching modes of Ti−O bonds that protrude into the interlayer space.[53] The low-frequency modes observed with the defects arise as a result of breaking of Ti−O bonds.

Figure 5 presents the dynamics of the electron loss. Assuming that the overall decay is exponential, as observed in

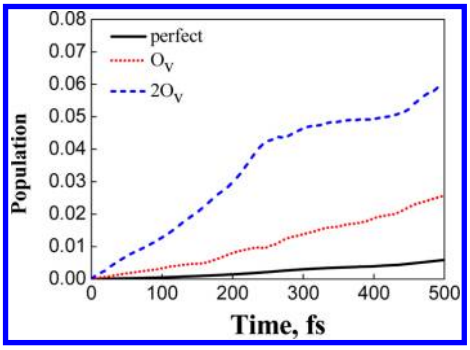

Figure 5. Evolution of the ground-state population due to nonradiative relaxation of the lowest energy electronic excitation in the TiO_2 nanotubes at 300 K. The perfect nanotube shows the slowest decay, while O_v defects accelerate the relaxation by as much as an order of magnitude (Table 1).

experiments, one can fit the 500 fs NAMD data with the expression $P(t) = 1 - \exp(t/\tau) \approx t/\tau$ and obtain the relaxation time τ. The nonradiative lifetime estimated for the perfect NT at ambient temperature is ~100 ps. The oxygen vacancies dramatically accelerate the relaxation, reducing the lifetime to <10 ps (Table 1). Our results agree with the time-resolved photoluminescence data for TiO_2 nanostructures.[54−56] The reported lifetimes are hundreds of picoseconds. The TiO_2 NT

dx.doi.org/10.1021/jz500565v | J. Phys. Chem. Lett. 2014, 5, 1642−1647

used here is significantly smaller than the NTs fabricated in the experiments. Small curvature NTs have large surface area and increased geometric strain and flexibility. Hence, the electron−phonon coupling in smaller diameter NTs is more sensitive to defects than that in bigger NTs. In addition, the small size of the simulation cell results in high defect concentration. Therefore, our simulations overestimate the relaxation time.

The nonradiative relaxation of defect states is difficult to study by optical measurements. Defects have low optical activity because the overlap between the localized defect states and the delocalized conduction and valence band states is small, and the corresponding transition dipole moments vanish. A small concentration of defects sites relative to bulk sites also hinders such measurements. Therefore, it is hard to establish whether the experimental data[54−56] describes electron trapping by defects or electron−hole recombination bypassing defects.

Both transition energy and electron−phonon coupling influence the relaxation process. The oxygen vacancy lowers the energy for the transition of the excited electron away from the conduction band, and a smaller transition energy favors faster nonradiative relaxation based on the energy gap law.[57] The NA electron−phonon coupling becomes 1.5 and 2 times larger in the NTs with one and two oxygen vacancies relative to the perfect NT (Table 1) because the defects localize the phonon modes and the electronic excitation. Local polar Ti−O vibrations created by the defect interact strongly with the local electron density (Figure 2). According to Fermi's golden rule, the relaxation rate depends on the square of the coupling. The order of the magnitude faster relaxation in the NT with two defects (Figure 5, Table 1) arises from a combination of the lower energy gap (Figure 3) and stronger electron−phonon coupling (Table 1).

It is valuable to compare the relaxation dynamics in the TiO_2 NTs to those in carbon NTs.[51] Defects enhance the relaxation in both TiO_2 and carbon NTs. The NA coupling in carbon NT originates from the overlap of the π-electron orbitals that extend perpendicularly to the tube. Defects break the π-bonding network, give rise to local electronic states and anharmonic vibrations, and accelerate the relaxation. Similarly, the Ti^{3+} defects break the periodicity of the TiO_2 conduction and valence band states, create local states and vibrational modes, and increase energy and charge losses.

To recapitulate, there exists a significant discrepancy between the expected and measured values of electron mobility for oriented polycrystalline titania NTs. To rationalize the discrepancy, we performed a time-domain, atomistic simulation of charge and energy losses in TiO_2 NTs with varying degree of oxygen-vacancy doping. We found that the vacancies created localized Ti^{3+} states 0.8 eV below the TiO_2 conduction band. The traps increased the electron-vibrational coupling. Higher defect concentration had minor influence on the trap state energy but enhanced the coupling further. By lowering the energy gap required for removal of the conducting electrons and by increasing the electron−phonon coupling, the traps accelerated the electron and energy losses by an order of magnitude, thus limiting the electron mobility. The energy relaxation in the perfect TiO_2 NT was facilitated by vibrations at 490 and 790 cm^{-1}. Polar low-frequency vibrations below 200 cm^{-1} were responsible for the losses in the NT with defects. The simulations clearly show that one can greatly enhance charge mobility in TiO_2 NTs and increase photovoltaic efficiencies by removing defects, such as oxygen vacancies, and improving NT crystallinity. The general conclusions of our work apply to other nanoscale and low-dimensional materials, such as carbon NTs, graphene, conjugated polymers, and so on.

AUTHOR INFORMATION

Corresponding Author

*E-mail: yyli@suda.edu.cn.

Notes

The authors declare no competing financial interests.

ACKNOWLEDGMENTS

The work is supported by the National Basic Research Program of China (973 Program, Grant No. 2012CB932400), the National Natural Science Foundation of China (Grant No. 91233115, 21273158, 21103118, and 91227201), and the Science Foundation of Ministry of Education of China (No: 20113201120020, 20133201110018), a Project Funded by the Priority Academic Program Development of Jiangsu Higher Education Institutions (PAPD). This is also a project supported by the Fund for Innovative Research Teams of Jiangsu Higher Education Institutions. O.V.P. acknowledges support of the U.S. Department of Energy, grant DE-SC0006527

REFERENCES

(1) Peter, L. M. The Gratzel Cell: Where Next? *J. Phys. Chem. Lett.* **2011**, *2* (15), 1861−1867.

(2) Oregan, B.; Gratzel, M. A Low-Cost, High-Efficiency Solar-Cell Based on Dye-Sensitized Colloidal TiO_2 Films. *Nature* **1991**, *353* (6346), 737−740.

(3) Gratzel, M. Recent Advances in Sensitized Mesoscopic Solar Cells. *Acc. Chem. Res.* **2009**, *42* (11), 1788−1798.

(4) Hagfeldt, A.; Boschloo, G.; Sun, L. C.; Kloo, L.; Pettersson, H. Dye-Sensitized Solar Cells. *Chem. Rev.* **2010**, *110* (11), 6595−6663.

(5) Gratzel, M. Dye-Sensitized Solar Cells. *J. Photochem. Photobiol., C* **2003**, *4* (2), 145−153.

(6) Yella, A.; Lee, H. W.; Tsao, H. N.; Yi, C. Y.; Chandiran, A. K.; Nazeeruddin, M. K.; Diau, E. W. G.; Yeh, C. Y.; Zakeeruddin, S. M.; Gratzel, M. Porphyrin-Sensitized Solar Cells with Cobalt (II/III)-Based Redox Electrolyte Exceed 12% Efficiency. *Science* **2011**, *334* (6056), 629−634.

(7) Burschka, J.; Pellet, N.; Moon, S. J.; Humphry-Baker, R.; Gao, P.; Nazeeruddin, M. K.; Gratzel, M. Sequential Deposition As a Route to High-Performance Perovskite-Sensitized Solar Cells. *Nature* **2013**, *499* (7458), 316−319.

(8) Jennings, J. R.; Ghicov, A.; Peter, L. M.; Schmuki, P.; Walker, A. B. Dye-Sensitized Solar Cells Based on Oriented TiO_2 Nanotube Arrays: Transport, Trapping, And Transfer of Electrons. *J. Am. Chem. Soc.* **2008**, *130* (40), 13364−13372.

(9) Ardo, S.; Meyer, G. J. Photodriven Heterogeneous Charge Transfer with Transition-Metal Compounds Anchored to TiO_2 Semiconductor Surfaces. *Chem. Soc. Rev.* **2009**, *38* (1), 115−164.

(10) Turner, G. M.; Beard, M. C.; Schmuttenmaer, C. A. Carrier Localization and Cooling in Dye-Sensitized Nanocrystalline Titanium Dioxide. *J. Phys. Chem. B* **2002**, *106* (45), 11716−11719.

(11) Gentilini, D.; Gagliardi, A.; Maur, M. A. D.; Vesce, L.; D'Ercole, D.; Brown, T. M.; Reale, A.; Di Carlo, A. Correlation between Cell Performance and Physical Transport Parameters in Dye Solar Cells. *J. Phys. Chem. C* **2012**, *116* (1), 1151−1157.

(12) Cai, J. H.; Han, L. Y. Theoretical Investigation on Interfacial-Potential-Limited Diffusion and Recombination in Dye-Sensitized Solar Cells. *J. Phys. Chem. C* **2011**, *115* (34), 17154−17162.

(13) Zhang, J.; Hughes, T. F.; Steigerwald, M.; Brus, L.; Friesner, R. A. Realistic Cluster Modeling of Electron Transport and Trapping in Solvated TiO_2 Nanoparticles. *J. Am. Chem. Soc.* **2012**, *134* (29), 12028−12042.

(14) Nunzi, F.; Mosconi, E.; Storchi, L.; Ronca, E.; Selloni, A.; Gratzel, M.; De Angelis, F. Inherent Electronic Trap States in TiO_2

Nanocrystals: Effect of Saturation and Sintering. *Energy Environ. Sci.* **2013**, *6* (4), 1221−1229.
(15) Deak, P.; Aradi, B.; Frauenheim, T. Quantitative Theory of the Oxygen Vacancy and Carrier Self-Trapping in Bulk TiO_2. *Phys. Rev. B* **2012**, *86* (19), 195206.
(16) Gong, D.; Grimes, C. A.; Varghese, O. K.; Hu, W. C.; Singh, R. S.; Chen, Z.; Dickey, E. C. Titanium Oxide Nanotube Arrays Prepared by Anodic Oxidation. *J. Mater. Res.* **2001**, *16* (12), 3331−3334.
(17) Xiong, H.; Slater, M. D.; Balasubramanian, M.; Johnson, C. S.; Rajh, T. Amorphous TiO_2 Nanotube Anode for Rechargeable Sodium Ion Batteries. *J. Phys. Chem. Lett.* **2011**, *2* (20), 2560−2565.
(18) Ferrari, A. M.; Szieberth, D.; Zicovich-Wilson, C. M.; Demichelis, R. Anatase(001) 3 ML Nanotubes, The First TiO_2 Nanotube With Negative Strain Energies: A DFT Prediction. *J. Phys. Chem. Lett.* **2010**, *1* (19), 2854−2857.
(19) Bavykin, D. V.; Friedrich, J. M.; Walsh, F. C. Protonated Titanates and TiO_2 Nanostructured Materials: Synthesis, Properties, And Applications. *Adv. Mater.* **2006**, *18* (21), 2807−2824.
(20) Zakharova, G. S.; Jahne, C.; Popa, A.; Taschner, C.; Gemming, T.; Leonhardt, A.; Buchner, B.; Klingeler, R. Anatase Nanotubes as an Electrode Material for Lithium-Ion Batteries. *J. Phys. Chem. C* **2012**, *116* (15), 8714−8720.
(21) Roy, P.; Berger, S.; Schmuki, P. TiO_2 Nanotubes: Synthesis and Applications. *Angew. Chem., Int. Ed.* **2011**, *50* (13), 2904−2939.
(22) Meekins, B. H.; Kamat, P. V. Got TiO_2 Nanotubes? Lithium Ion Intercalation Can Boost Their Photoelectrochemical Performance. *ACS Nano* **2009**, *3* (11), 3437−3446.
(23) Varghese, O. K.; Paulose, M.; Grimes, C. A. Long Vertically Aligned Titania Nanotubes on Transparent Conducting Oxide for Highly Efficient Solar Cells. *Nat. Nanotechnol.* **2009**, *4* (9), 592−597.
(24) Mor, G. K.; Varghese, O. K.; Paulose, M.; Shankar, K.; Grimes, C. A. A Review on Highly Ordered, Vertically Oriented TiO_2 Nanotube Arrays: Fabrication, Material Properties, and Solar Energy Applications. *Sol. Energy Mater. Sol. Cells* **2006**, *90* (14), 2011−2075.
(25) Varghese, O. K.; Paulose, M.; LaTempa, T. J.; Grimes, C. A. High-Rate Solar Photocatalytic Conversion of CO_2 and Water Vapor to Hydrocarbon Fuels. *Nano Lett.* **2009**, *9* (2), 731−737.
(26) Zhu, K.; Neale, N. R.; Miedaner, A.; Frank, A. J. Enhanced Charge-Collection Efficiencies and Light Scattering in Dye-Sensitized Solar Cells Using Oriented TiO_2 Nanotubes Arrays. *Nano Lett.* **2007**, *7* (1), 69−74.
(27) Richter, C.; Schmuttenmaer, C. A. Exciton-Like Trap States Limit Electron Mobility in TiO_2 Nanotubes. *Nat. Nanotechnol.* **2010**, *5* (11), 769−772.
(28) Neukirch, A. J.; Guo, Z. Y.; Prezhdo, O. V. Time-Domain Ab Initio Study of Phonon-Induced Relaxation of Plasmon Excitations in a Silver Quantum Dot. *J. Phys. Chem. C* **2012**, *116* (28), 15034−15040.
(29) Tully, J. C. Molecular-Dynamics with Electronic-Transitions. *J. Chem. Phys.* **1990**, *93* (2), 1061−1071.
(30) Craig, C. F.; Duncan, W. R.; Prezhdo, O. V. Trajectory Surface Hopping in the Time-Dependent Kohn-Sham Approach for Electron-Nuclear Dynamics. *Phys. Rev. Lett.* **2005**, *95* (16), 163001.
(31) Fischer, S. A.; Habenicht, B. F.; Madrid, A. B.; Duncan, W. R.; Prezhdo, O. V. Regarding the Validity of the Time-Dependent Kohn-Sham Approach for Electron-Nuclear Dynamics via Trajectory Surface Hopping. *J. Chem. Phys.* **2011**, *134* (2), 024102.
(32) Duncan, W. R.; Craig, C. F.; Prezhdo, O. V. Time-Domain Ab Initio Study of Charge Relaxation and Recombination in Dye-Sensitized TiO_2. *J. Am. Chem. Soc.* **2007**, *129* (27), 8528−8543.
(33) Long, R.; Prezhdo, O. V. Ab Initio Nonadiabatic Molecular Dynamics of the Ultrafast Electron Injection from a PbSe Quantum Dot into the TiO_2 Surface. *J. Am. Chem. Soc.* **2011**, *133* (47), 19240−19249.
(34) Long, R.; English, N. J.; Prezhdo, O. V. Photo-Induced Charge Separation across the Graphene-TiO_2 Interface Is Faster than Energy Losses: A Time-Domain ab Initio Analysis. *J. Am. Chem. Soc.* **2012**, *134* (34), 14238−14248.
(35) Habenicht, B. F.; Prezhdo, O. V. Ab Initio Time-Domain Study of the Triplet State in a Semiconducting Carbon Nanotube: Intersystem Crossing, Phosphorescence Time, and Line Width. *J. Am. Chem. Soc.* **2012**, *134* (38), 15648−15651.
(36) Habenicht, B. F.; Prezhdo, O. V. Time-Domain Ab Initio Study of Nonradiative Decay in a Narrow Graphene Ribbon. *J. Phys. Chem. C* **2009**, *113* (32), 14067−14070.
(37) Nelson, T. R.; Prezhdo, O. V. Extremely Long Nonradiative Relaxation of Photoexcited Graphane Is Greatly Accelerated by Oxidation: Time-Domain Ab Initio Study. *J. Am. Chem. Soc.* **2013**, *135* (9), 3702−3710.
(38) Kresse, G.; Furthmuller, J. Efficient Iterative Schemes for Ab Initio Total-Energy Calculations Using a Plane-Wave Basis Set. *Phys. Rev. B* **1996**, *54* (16), 11169−11186.
(39) Perdew, J. P.; Burke, K.; Ernzerhof, M. Generalized Gradient Approximation Made Simple. *Phys. Rev. Lett.* **1996**, *77* (18), 3865−3868.
(40) Blochl, P. E. Projector Augmented-Wave Method. *Phys. Rev. B* **1994**, *50* (24), 17953−17979.
(41) Kresse, G.; Joubert, D. From Ultrasoft Pseudopotentials to the Projector Augmented-Wave Method. *Phys. Rev. B* **1999**, *59* (3), 1758−1775.
(42) Becke, A. D. Density-Functional Thermochemistry 0.3. The Role of Exact Exchange. *J. Chem. Phys.* **1993**, *98* (7), 5648−5652.
(43) Heyd, J.; Scuseria, G. E.; Ernzerhof, M. Hybrid Functionals Based on a Screened Coulomb Potential. *J. Chem. Phys.* **2003**, *118* (18), 8207−8215.
(44) Anisimov, V. I.; Zaanen, J.; Andersen, O. K. Band Theory and Mott Insulators - Hubbard-U Instead of Stoner-I. *Phys. Rev. B* **1991**, *44* (3), 943−954.
(45) Zhao, Y. F.; Hou, T. J.; Li, Y. Y.; Chan, K. S.; Lee, S. T. Effective Increasing of Optical Absorption of TiO_2 by Introducing Trivalent Titanium. *Appl. Phys. Lett.* **2013**, *102* (17).
(46) Yu, X. H.; Hou, T. J.; Li, Y. Y.; Sun, X. H.; Lee, S. T. Effective Band Gap Reduction of Titanium Oxide Semiconductors by Codoping from First-Principles Calculations. *Int. J. Quantum Chem.* **2013**, *113* (23), 2546−2553.
(47) Yu, X. H.; Hou, T. J.; Sun, X. H.; Li, Y. Y. The Influence of Defects on Mo-Doped TiO_2 by First-Principles Studies. *ChemPhysChem* **2012**, *13* (6), 1514−1521.
(48) Deskins, N. A.; Rousseau, R.; Dupuis, M. Distribution of Ti3+ Surface Sites in Reduced TiO_2. *J. Phys. Chem. C* **2011**, *115* (15), 7562−7572.
(49) Kowalski, P. M.; Camellone, M. F.; Nair, N. N.; Meyer, B.; Marx, D. Charge Localization Dynamics Induced by Oxygen Vacancies on the TiO_2(110) Surface. *Phys. Rev. Lett.* **2010**, *105* (14).
(50) Thomas, A. G.; Flavell, W. R.; Mallick, A. K.; Kumarasinghe, A. R.; Tsoutsou, D.; Khan, N.; Chatwin, C.; Rayner, S.; Smith, G. C.; Stockbauer, R. L.; Warren, S.; Johal, T. K.; Patel, S.; Holland, D.; Taleb, A.; Wiame, F. Comparison of the Electronic Structure of Anatase and Rutile TiO_2 Single-Crystal Surfaces Using Resonant Photoemission and X-ray Absorption Spectroscopy. *Phys. Rev. B* **2007**, *75* (3), 146405.
(51) Habenicht, B. F.; Prezhdo, O. V. Nonradiative Quenching of Fluorescence in a Semiconducting Carbon Nanotube: A Time-Domain Ab Initio Study. *Phys. Rev. Lett.* **2008**, *100* (19).
(52) Balachandran, U.; Eror, N. G. Raman-Spectra of Titanium-Dioxide. *J. Solid State Chem.* **1982**, *42* (3), 276−282.
(53) Ma, R.; Fukuda, K.; Sasaki, T.; Osada, M.; Bando, Y. Structural Features of Titanate Nanotubes/Nanobelts Revealed by Raman, X-ray Absorption Fine Structure and Electron Diffraction Characterizations. *J. Phys. Chem. B* **2005**, *109* (13), 6210−6214.
(54) Dillon, R. J.; Joo, J. B.; Zaera, F.; Yin, Y. D.; Bardeen, C. J. Correlating the Excited State Relaxation Dynamics As Measured by Photoluminescence and Transient Absorption with the Photocatalytic Activity of Au@TiO_2 Core-Shell Nanostructures. *Phys. Chem. Chem. Phys.* **2013**, *15* (5), 1488−1496.
(55) Fujihara, K.; Izumi, S.; Ohno, T.; Matsumura, M. Time-Resolved Photoluminescence of Particulate TiO_2 Photocatalysts Suspended in Aqueous Solutions. *J. Photochem. Photobiol., A* **2000**, *132* (1−2), 99−104.

(56) Wang, X. L.; Feng, Z. C.; Shi, J. Y.; Jia, G. Q.; Shen, S. A.; Zhou, J.; Li, C. Trap States and Carrier Dynamics of TiO_2 Studied by Photoluminescence Spectroscopy under Weak Excitation Condition. *Phys. Chem. Chem. Phys.* **2010**, *12* (26), 7083−7090.
(57) Englman, R.; Jortner, J. Energy Gap Law for Radiationless Transitions in Large Molecules. *Mol. Phys.* **1970**, *18* (2), 145−164.